Supplementary Table S1. NMR experimental restraints and structural statistics for the 10 lowest energy structures of DenvBS (bottom helix)

	DenvBS
NMR Peak Assignment (excluding the unstructured 5'-tail, nucleotides 1-5)	
All H1′, H2′, H5, H6, H8, AdeH2, 87.5% of H3', 59.4% of H4' and 18.8% of H5'/H5'' were assigned. Extensive overlap in the sugar proton region was relieved by deuteration of H3', H4', H5', H5 ''and H5 protons to assign H1' and H2' unambiguously, but this prevented assignments of many of those sugar protons. 63.2% of imino protons and 85.7% of Cyt amino protons were assigned.	
NMR Experimental Restraints	
Total number of restraints	539
Total NOE Restraints	299
Intra-residue	162
Inter-residue	137
Sequential |i-j| = 1	116
Non-sequential |i-j| > 1	21
Hydrogen bond restraints	10
Dihedral Angle Restraints[(a)]	216
Planarity Restraints	24
Structure Analysis	
NOE violations >0.5 Å	0
Torsion angle violations >5°	0
Deviation from Idealized Geometry	
RMS Deviation of Bond lengths (Å)	0.00
RMS Deviation of Bond angles (°)	0.63
Heavy Atom RMSD to the Mean Structure (Å)	
All RNA heavy atoms (6-36, excluding the unstructured 5'-tail)	1.02
All RNA backbone (6-36, excluding the unstructured 5'-tail)	1.00
RNA upper stem heavy atoms (13-28)	0.72
RNA upper stem backbone (13-28)	0.60
RNA lower stem heavy atoms (6-12, 29-36)	0.50
RNA lower stem backbone (6-12, 29-36)	0.53

(a) Generic dihedral restraints were applied to A-form helical regions confirmed by NOESY spectra.

Supplementary Table S2. NMR experimental restraints and structural statistics for the 10 lowest energy structures of DenvTSL (apical stem-loop)

	DenvTSL
NMR Peak Assignment	
All H1′, H2′, H5, H6, H8, and 25% of AdeH2[(a)], 92.9% of H3', 67.9% of H4' and 37.5% of H5'/H5'' were assigned. Extensive overlap in the sugar proton region was relieved by deuteration of H3', H4', H5', H5 '' and H5 protons to assign H1' and H2' unambiguously, but this prevented assignment of many of those deuterated sugar protons. 58.3% of imino protons and 75% of Cyt amino protons were assigned.	
NMR Experimental Restraints	
Total number of restraints	475
Total NOE Restraints	251
Intra-residue	135
Inter-residue	116
Sequential |i-j| = 1	92
Non-sequential |i-j| > 1	24
Hydrogen bond restraints	9
Dihedral Angle Restraints[(b)]	206
Planarity Restraints	18
Structure Analysis	
NOE violations >0.5 Å	0
Torsion angle violations >5°	0
RMS Deviation from Idealized Geometry	
RMS Deviation of Bond lengths (Å)	0.00
RMS Deviation of Bond angles (°)	0.64
Heavy Atom RMSD to the Mean Structure (Å)	
All RNA heavy atoms (1-28)	0.85
All RNA backbone (1-28)	0.75
RNA upper stem heavy atoms (7-22)	1.03
RNA upper stem backbone (7-22)	0.84

(a) H2 of Adenines located in single-stranded loops were not assigned.
(b) Generic dihedral restraints were applied to A-form helical regions confirmed by NOESY spectra.

Supplementary Table S3. NMR experimental restraints and structural statistics for the 10 lowest energy structures of DenvSLAsh (three-way junction)

	DenvSLAsh
NMR Peak Assignment	
90% of H1′, 95% of H2′, 94.1% of H5, 97.5% of H6/H8, 47.5% of H3', 27.5% of H4', 16.3% of H5'/H5'' and 40% of AdeH2[(a)] were assigned. Extensive overlap in the sugar proton region was relieved by deuteration of H3', H4', H5', H5 ''and H5 protons to assign H1' and H2' unambiguously, but this prevented assignments of many of those deuterated sugar protons. 65% of imino protons and 80% of Cyt amino protons were assigned.	
NMR Experimental Restraints	
Total number of restraints	840
Total NOE Restraints	562
Intra-residue	262
Inter-residue	300
Sequential |i-j| = 1	187
Non-sequential |i-j| > 1	113
Hydrogen bond restraints	41
Dihedral Angle Restraints[(b)]	250
Planarity Restraints	28
Structure Analysis	
NOE violations >0.5 Å	0
Torsion angle violations >5º	0
Deviation from Idealized Geometry	
RMS Deviation of Bond lengths (Å)	0.00
RMS Deviation of Bond angles (º)	0.68
Heavy Atom RMSD to the Mean Structure (Å)	
All RNA heavy atoms (1-40)	2.75[(c)]
All RNA backbone (1-40)	2.67[(c)]
RNA top and side stem heavy atoms (10-33)	2.07
RNA top and side stem backbone (10-33)	1.88
RNA bottom stem heavy atoms (1-9, 34-40)	1.76
RNA bottom stem backbone (1-9, 34-40)	1.11

(a) H2 of Adenines located in single-stranded loop were not assigned.
(b) Generic dihedral restraints were applied to A-form helical regions confirmed by NOESY spectra.

Supplementary Table S4. NMR experimental restraints and structural statistics for the 10 lowest energy structures of DenvSLATL (full-length monomeric SLA)

	DenvSLATL
NMR Experimental Restraints[a]	
Total number of restraints	1277
Total NOE Restraints	843
Intra-residue	402
Inter-residue	441
Sequential |i-j| = 1	303
Non-sequential |i-j| > 1	138
Hydrogen bond restraints	68
Dihedral Angle Restraints	384
Planarity Restraints	50
Structure Analysis	
NOE violations >0.5 Å	0
Torsion angle violations >5°	0
Deviation from Idealized Geometry	
RMS Deviation of Bond lengths (Å)	0.00
RMS Deviation of Bond angles (°)	0.66
Heavy Atom RMSD to the Mean Structure (Å)	
All RNA heavy atoms (6-70)	3.98[b][c]
All RNA backbone (6-70)	4.08[b][c]
Top stemloop heavy atoms (22-45, corresponding to DenvTSL)	1.33
Top stemloop backbone (22-45, corresponding to DenvTSL)	1.26
Bottom stem heavy atoms (6-18, 57-70, corresponding to DenvBS)	1.02
Bottom stem backbone (6-18, 57-70, corresponding to DenvBS)	1.00
Three-way junction heavy atoms (15-25, 42-60, corresponding to DenvSLAsh)	2.68
Three-way junction backbone (15-25, 42-60, corresponding to DenvSLAsh)	2.68

(a) Experimental restraints were derived from structural segments DenvBS, DenvTSL and DenvSLAsh (as described in Materials and Methods).
(b) The RMSD is calculated without the unstructured single-stranded 5'-tail (residues 1-5).

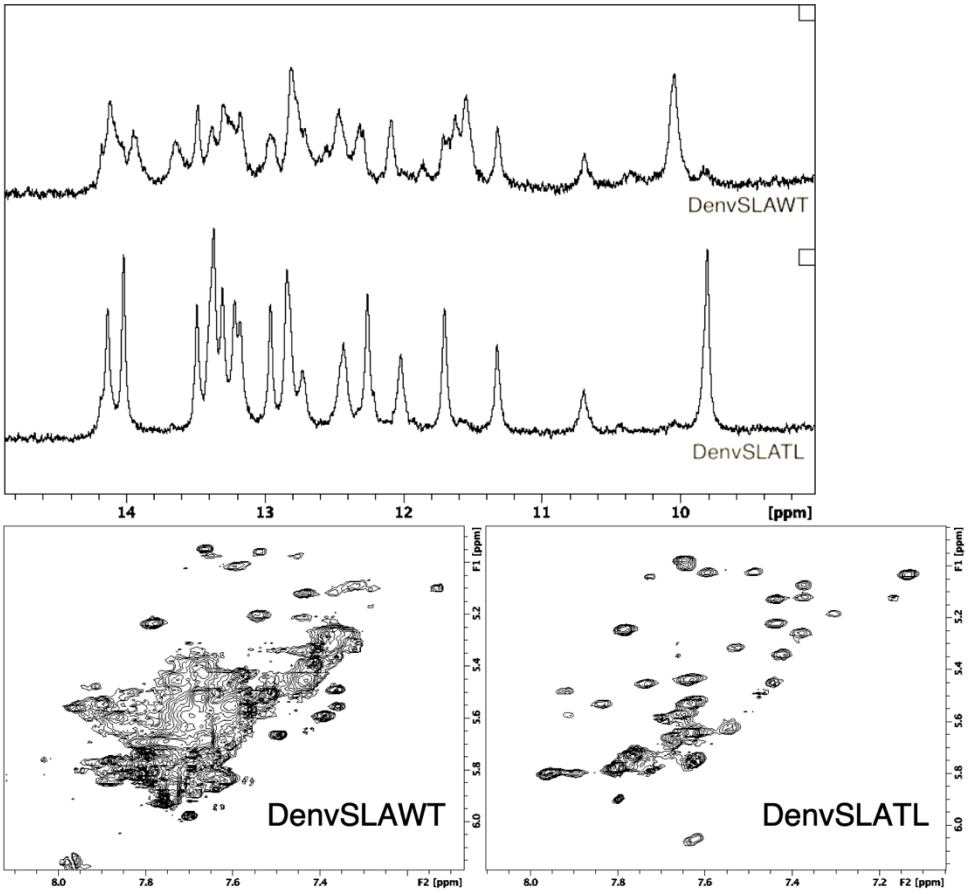

Supplementary Figure S1. (A) Comparison of the imino region of the 1D ^{1}H spectra of wild-type DENV1 SLA (called DenvSLAWT) and a UUCG-tetraloop-stabilized SLA promoter (called DenvSLATL). The addition of stabilizing tetraloops has been observed to improve linewidth with multiple RNAs we studied in the past, and was also observed in this case. The spectra of DenvSLAWT and DenvSLATL are similar, but the quality is much higher for the tetraloop-containing RNA with less overlaps and well-separated peaks. This is also in part caused by the partial dimerization of the wide-type RNA through the side stem-loop at the mM concentrations of NMR experiments, which would further increase the linewidth and the number of peaks in the spectrum. (B) Comparison of the H5-H6 region of the 2D TOCSY spectra of wild-type (DenvSLAWT) and tetraloop-stabilized SLA (DenvSLATL). While many of the peaks are in similar locations, the spectra for DenvSLAWT have much broader linewidth resulting in severe peak overlaps, which would make peak assignments extremely difficult. The addition of tetraloops improves linewidth and allows identification of discrete

peaks, as we have observed with multiple RNAs in the past (Barnwal et al., 2016; Sharma & Varani, 2020; Walker et al., 2020). This strategy is analogous to what is often done in crystallography, where crystallization modules (e.g. protein binding sites) are introduced to facilitate crystal packing and increase resolution.

Name	Length	Sequence
DenvSLAWT	70	GGAGU UGUUA GUCUA CGUGG ACCGA CAAGA ACAGU UUCGA AUCGG AAGCU UGCUU AACGU AGUUC UAACA
DenvSLATL	70	GGAGU GGUUA GUCUA CGUGG ACCGA CAAGA CUUCG GUCGA AUCGG AAGGA AACUU AACGU AGUUC UAACC
DenvBS	36	GGAGU GGUUA GUCUA CGUUU CGACG UAGUU CUAAC C
DenvTSL	28	GGCCG ACAAG AACAG UUUCG AAUCG GCC
DenvSLAsh	40	GGACG UGGAC CGACU UCGGU CGGAA GGAAA CUUAA CGUCC
SLAshCUUG	40	GGACG UGGAC CGACU UCGGU CGGAA GCUUG CUUAA CGUCC

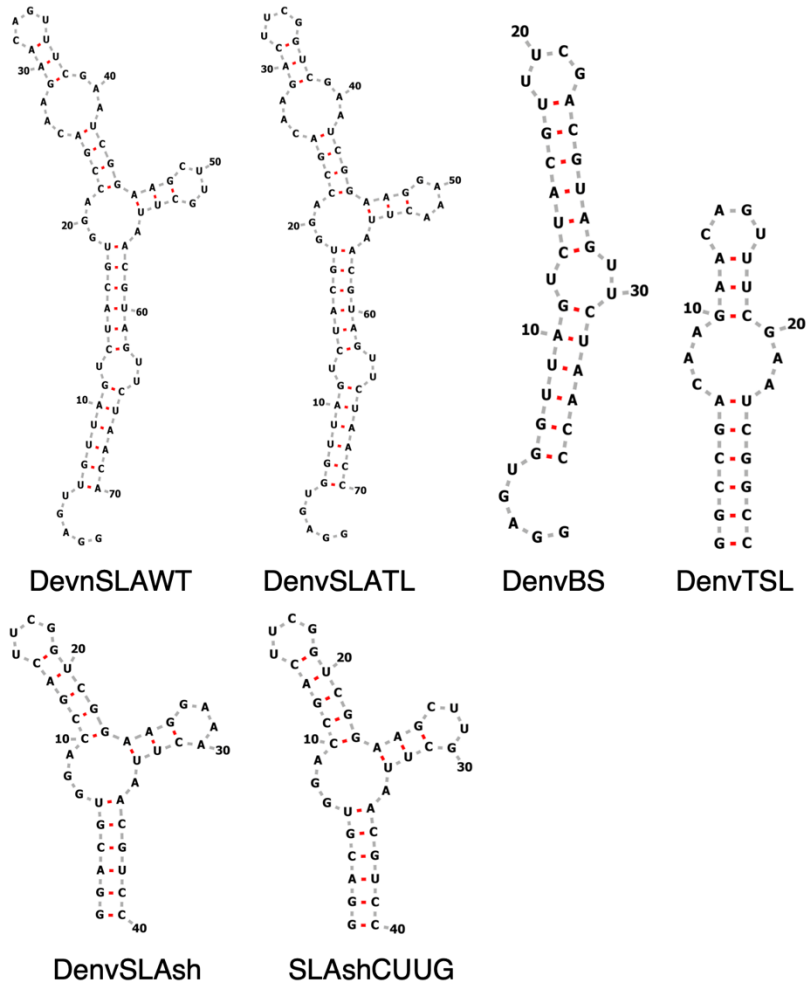

Supplementary Figure S2. Sequences and secondary structures of all RNAs studied in this work; all secondary structures were verified by NMR assignments of NH resonances.

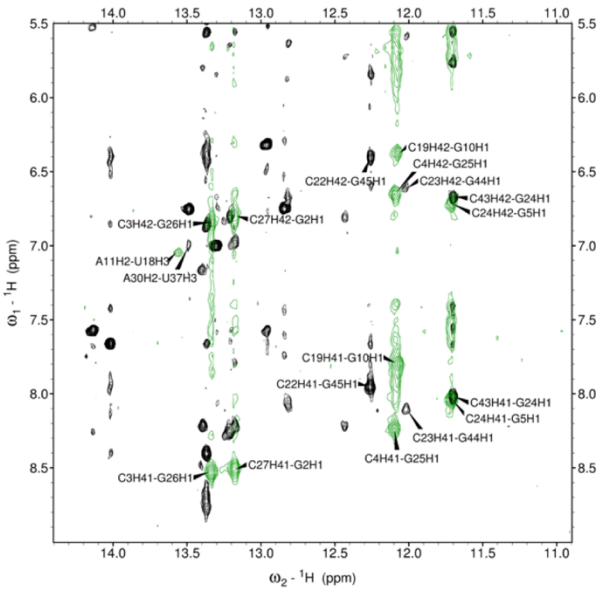

DenvTSL

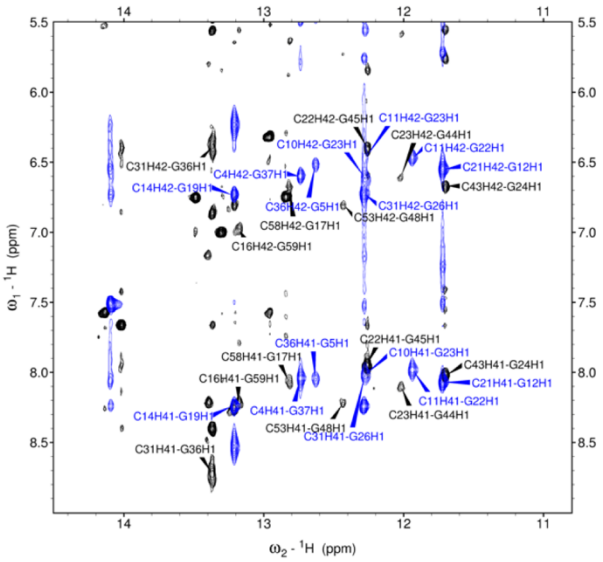

DenvSLAsh

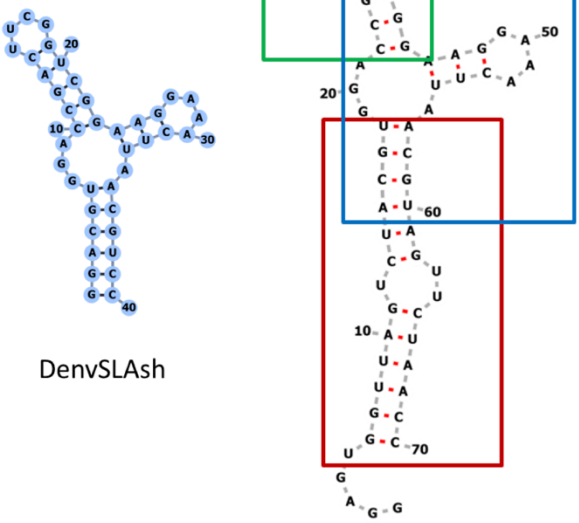

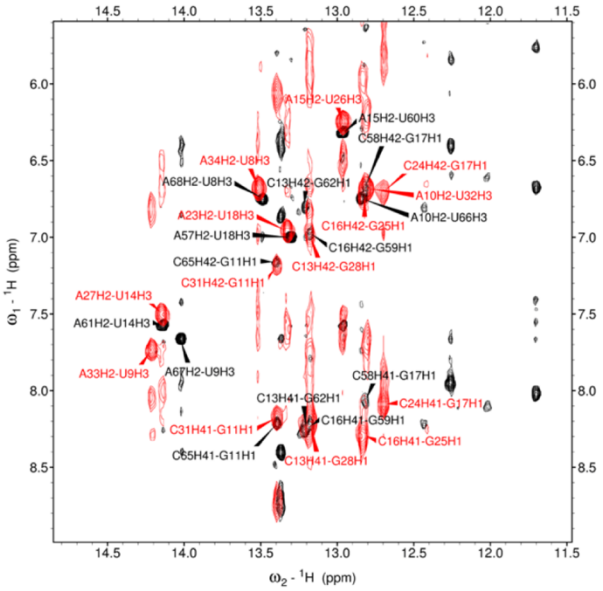

DenvBS

Supplementary Figure S3. Overlay of the imino region of NOESY spectra for DenvSLATL (black) to DenvBS (red), DenvSLAsh (blue), and DenvTSL (green). Assignments for each RNA are shown in the corresponding color. High similarity of chemical shifts and NOE patterns were observed in each segment; thus, assignments for DenvSLATL were safely transferred from each corresponding segment.

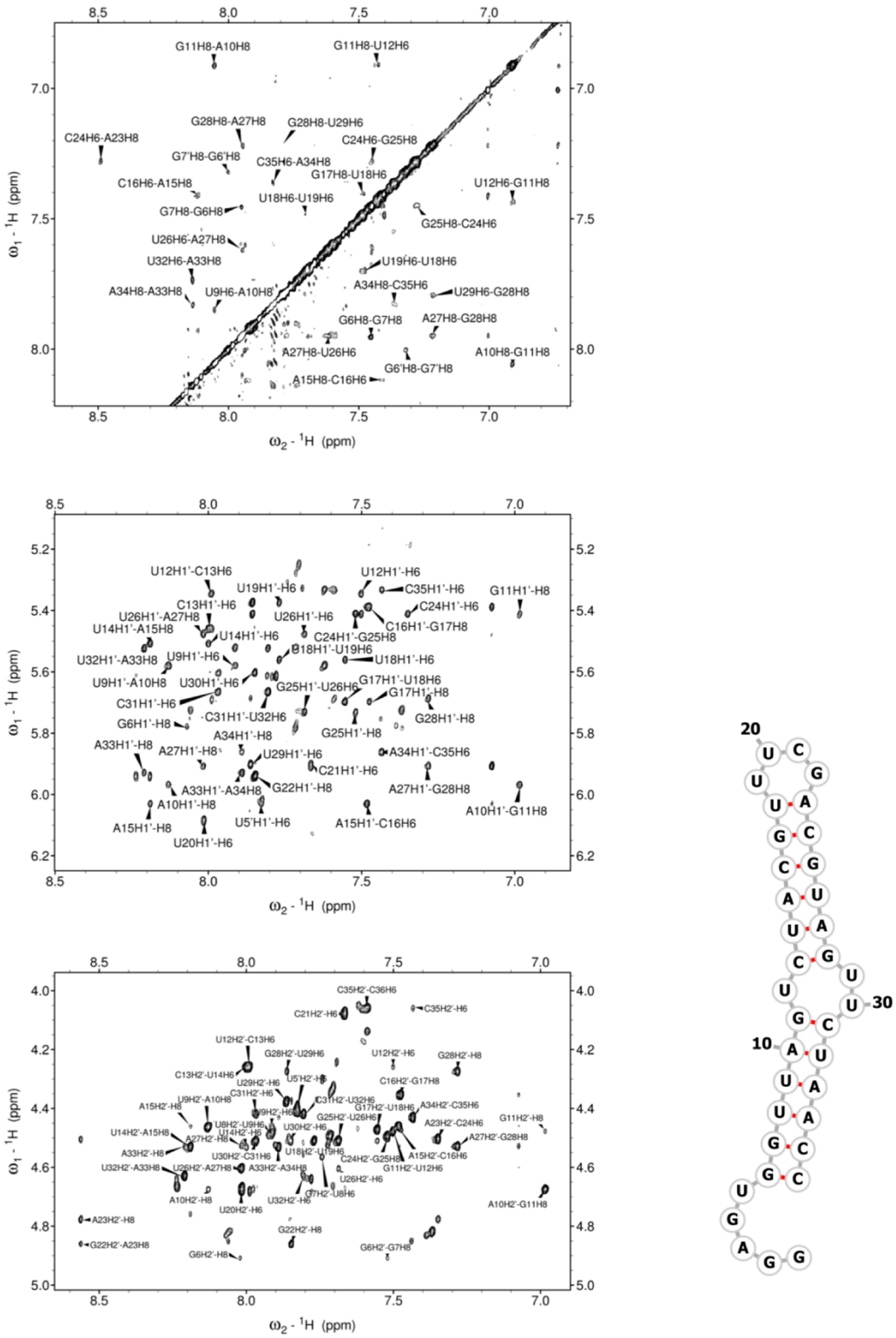

Supplementary Figure S4. NOESY spectra of non-exchangeable proton region (H6/H8-H6/H8 and sugar proton-H6/H8) for DenvBS; the secondary structure is shown on the right. Deuteration of H5, H3', H4', H5', H5'' protons relieved the extensive overlap in the sugar proton region.

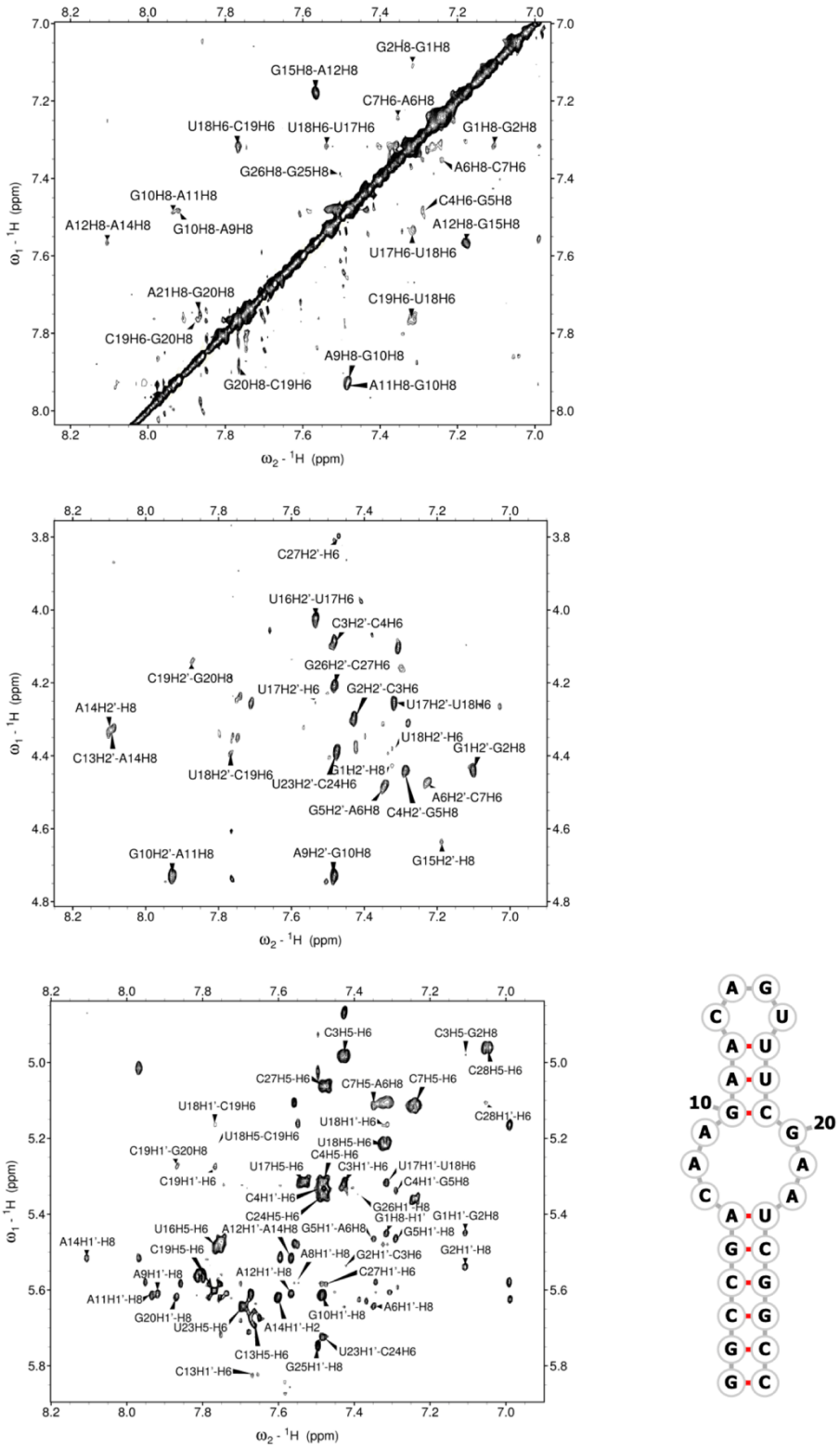

Supplementary Figure S5. NOESY spectra of non-exchangeable proton region (H6/H8-H6/H8 and sugar proton-H6/H8) for DenvTSL; the secondary structure is shown on the right. Deuteration of H5, H3', H4', H5', H5'' protons relieved the extensive overlap in the sugar proton region.

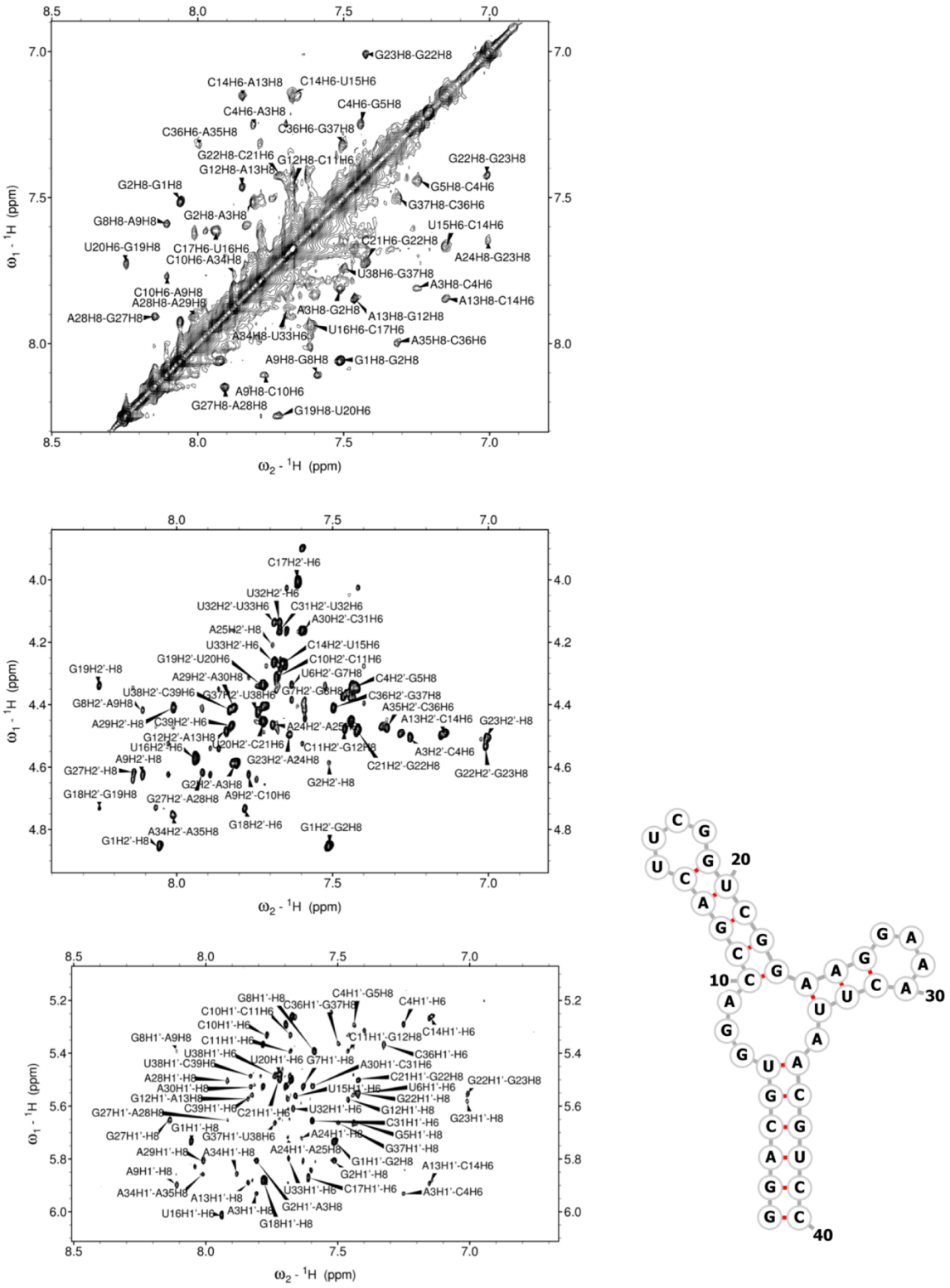

Supplementary Figure S6. NOESY spectra of non-exchangeable proton region (H6/H8-H6/H8 and sugar proton-H6/H8) for DenvSLAsh; the secondary structure is shown on the right. Deuteration of H5, H3', H4', H5', H5'' protons relieved the extensive overlap in the sugar proton region.

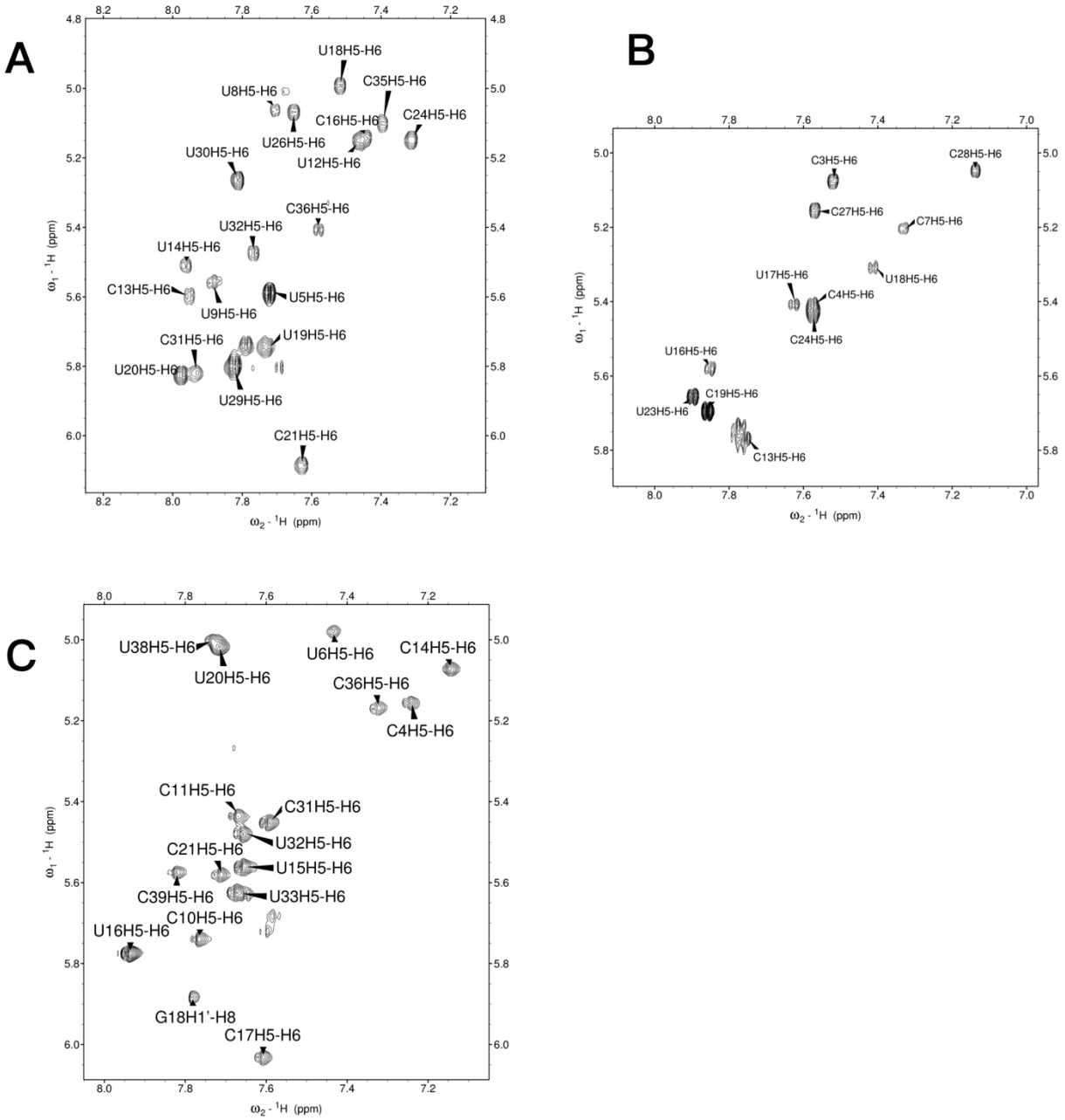

Supplementary Figure S7. TOCSY spectra for the three independently folded structural segments: (A) DenvBS, (B) DenvTSL, and (C) DenvSLAsh. The existence of a single monomeric conformation for each RNA was confirmed from the number of Ura and Cyt H5-H6 peaks in TOCSY spectra, which was as predicted for each sequence.

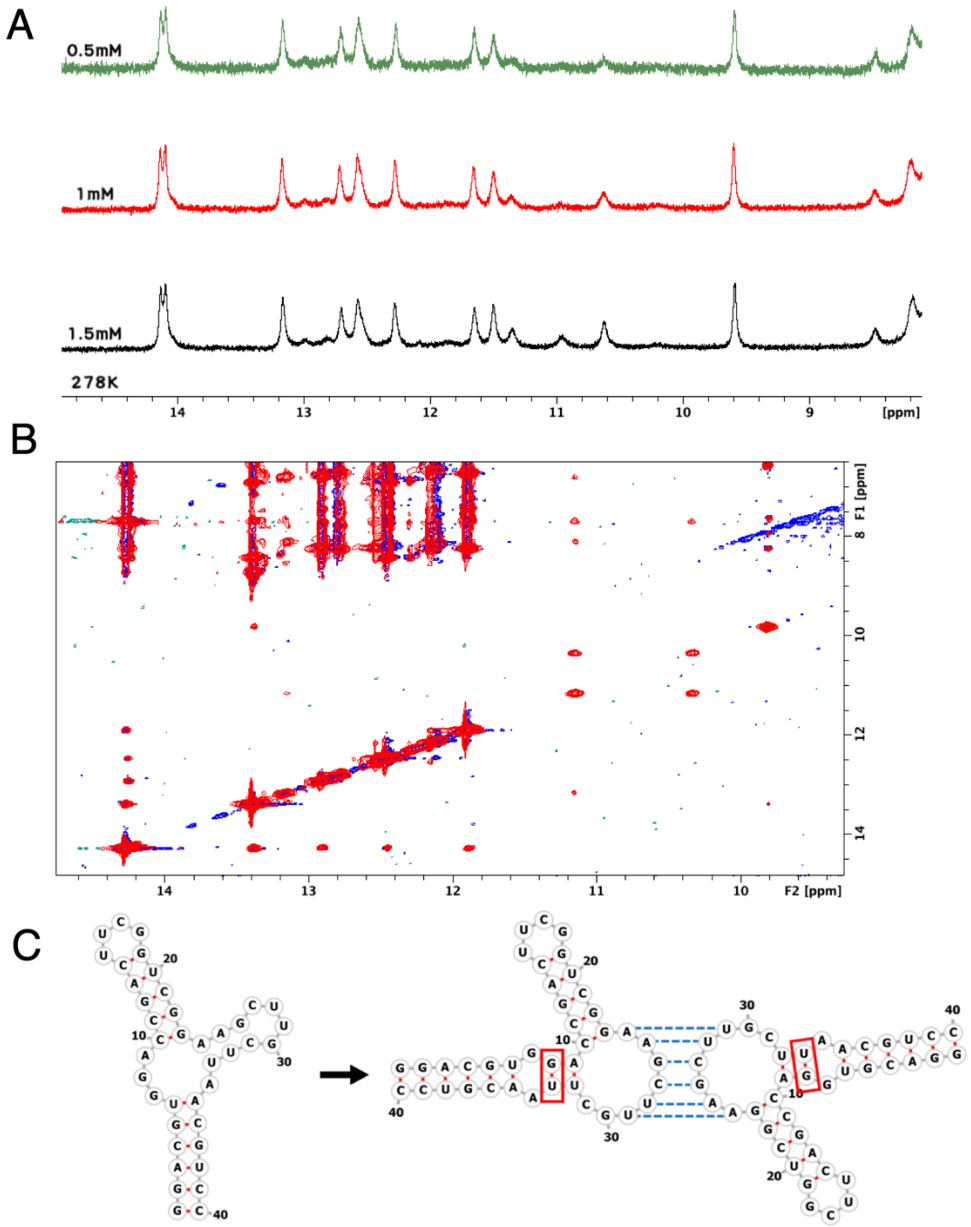

Supplementary Figure S8. (A) 1D ^{1}H NMR spectra of SLAshCUUG recorded at 5°C at concentrations of 0.5 mM (green), 1 mM (red), and 1.5 mM (black). Concentration-dependent peaks are observed between 10-12 ppm and between 12 and 13 ppm, which imply formation of new base pairs as a result of dimerization, which of course becomes more favorable at higher RNA concentration. (B) Overlay of 2D ^{1}H NOESY spectra for SLAshCUUG (red) and DenvSLAsh (blue). For SLAshCUUG, extra base pair peaks are observed between 10-11 ppm, consistent with formation of a GU base pair. By substituting CUUG with a GAAA tetraloop, the extra resonances are eliminated. Peaks corresponding to base pairs in the side stem were not observed in the spectra of SLAshCUUG, implying

that the secondary structure of the side stem is likely to be unstable. (C) Secondary structures of the SLAshCUUG monomer and the presumed SLAshCUUG dimer. The secondary structure we show corresponds to the dimer observed in the crystal structure (Lee et al., 2021) and contains a GU base pair.

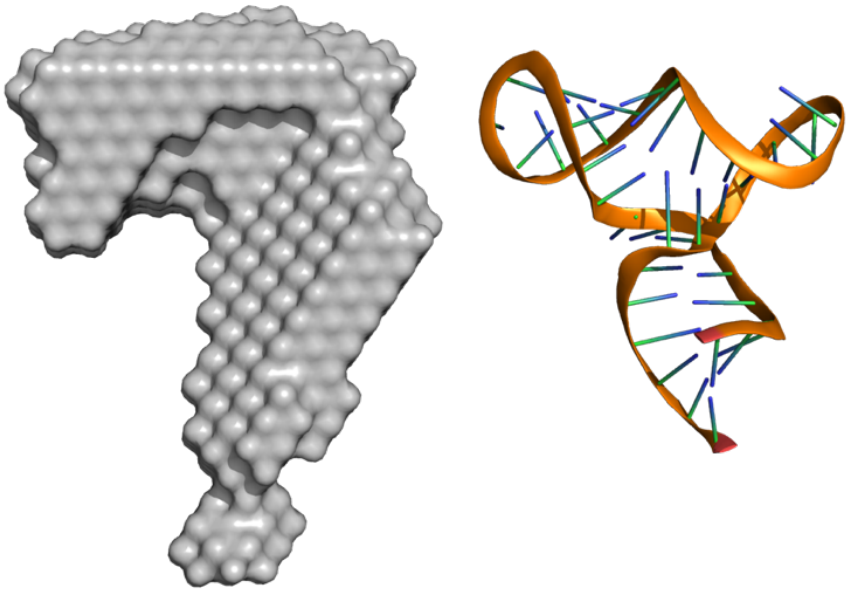

Supplementary Figure S9. The SAXS model of SLAshCUUG demonstrates a monomeric structure at concentrations below those used for NMR. Data was collected using the same process described in Method at RNA concentrations of 0.1-2 mg/mL. The structure of DenvSLAsh is shown on the right for comparison.

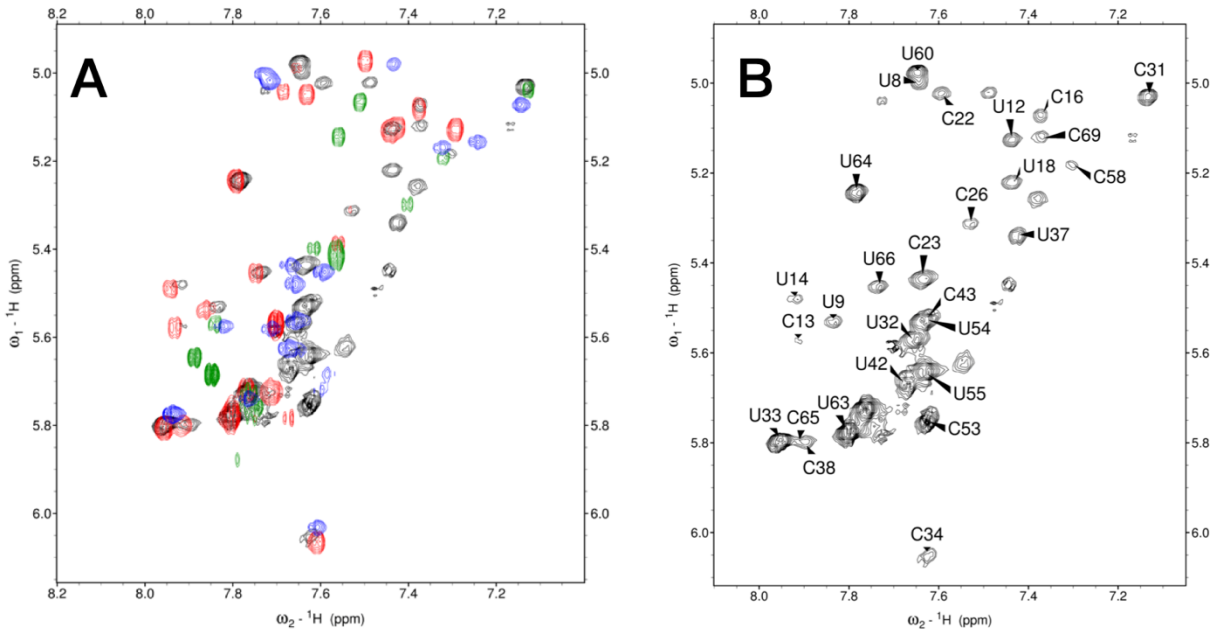

Supplementary Figure S10. (A) Overlay of the TOCSY spectra for DenvSLATL (black), DenvBS (red), DenvTSL (green) and DenvSLAsh (blue). The similarity of chemical shifts allowed us to assign H5-H6 cross-peaks for DenvSLATL, as shown. (B) H5-H6 peak assignments for the TOCSY spectrum of the complete DenvSLATL. A single dominant monomeric conformation was confirmed from the number of Ura and Cyt H5-H6 peaks in TOCSY spectra, which was consistent with its sequence.

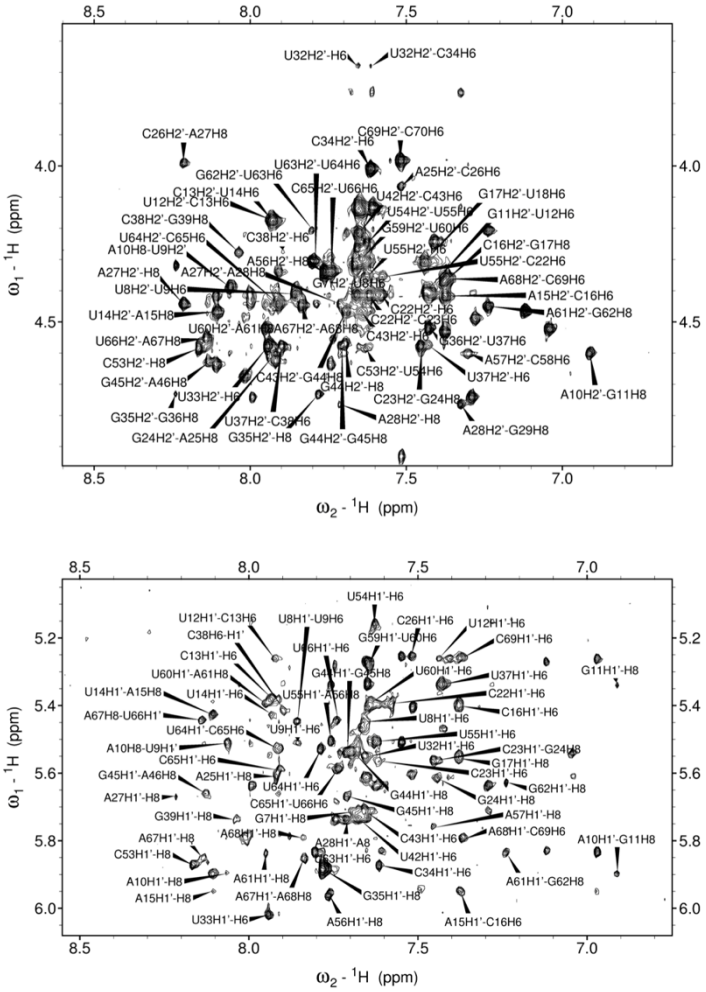

Supplementary Figure S11. NOESY spectra of the H1'-H6/H8 and H2'-H6/H8 region for DenvSLATL. Selective deuteration of H5, H3', H4', H5', H5'' protons was applied to relieve the extensive overlap in the sugar proton region, leading to interpretable and fully assignable spectra.

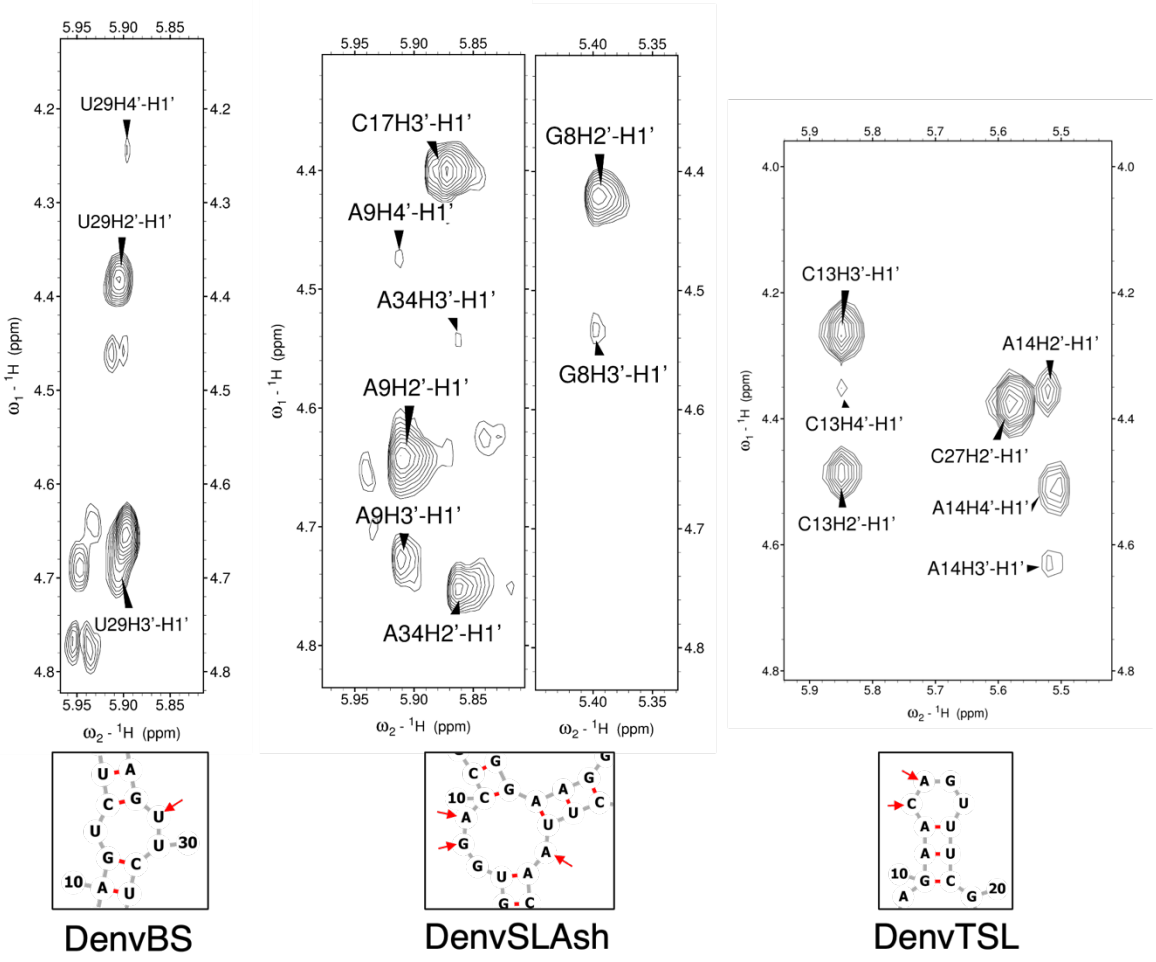

Supplementary Figure S12. Sugar proton region of TOCSY spectra of DenvBS, DenvSLAsh and DenvTSL. For 3'-endo sugar pucker, no peak is observable because the couplings are small; 2'-endo conformation has strong H1'-H2', medium H1'-H3' peaks and very weak/unobservable H1'-H4' peaks. For a mixture of 3' and 2'-endo conformations, peaks from H1' to H2', H3' and H4' are observed. According to the TOCSY spectra, Ura29 within the U-bulge, Ade9 and Gua8 in the three-way junction and the Cytosine in the upper loop have 2'-endo conformations. We cannot say anything about Ade34 because of spectral overlap around 4.4 ppm. Only the Ade in the apical loop occupies a mixture of 2' and 3'-endo conformations, which implies a dynamic structure for this nucleotide.

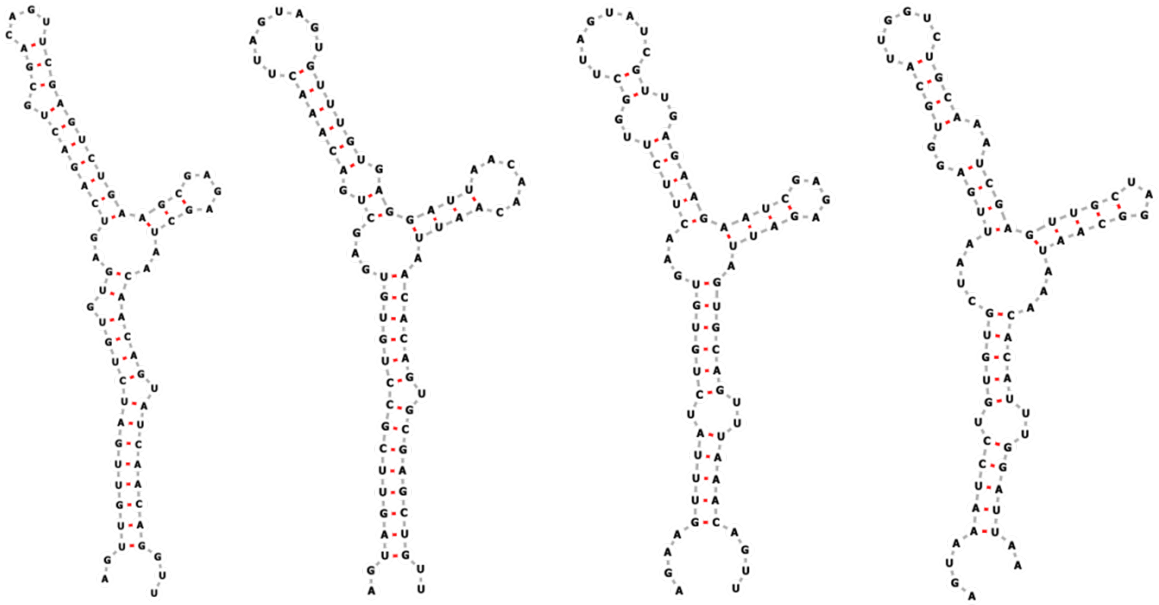

Supplementary Figure S13. Predicted SLA secondary structures, according to Vienna fold, for different flaviviruses (Lodeiro et al., 2009; Markham & Zuker, 2008; Zuker, 2003). Results are shown for Zika virus (NC_012532, nucleotide 1-106), West Nile virus (NC_001563, nucleotide 1-96), Japanese encephalitis virus (NC_001437, nucleotide 1-95), and Yellow fever virus (NC_002031, nucleotide 1-118).

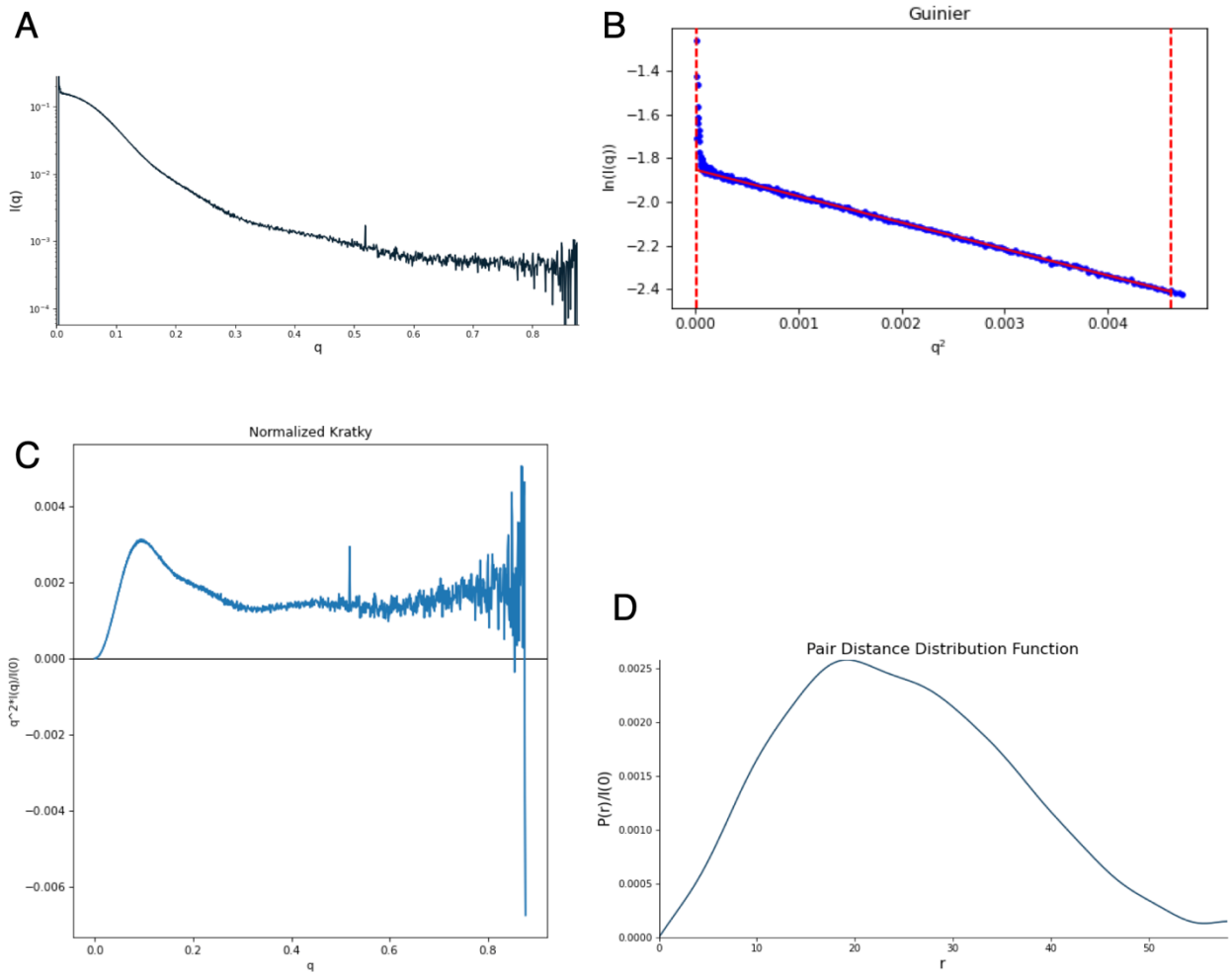

Supplementary Figure S14. Processed SAXS data of DenvSLAsh: (A) scattering curve, (B) Guinier approximation curve; (C) normalized Kratky plot; and (D) particle distance distribution function plot. The radius of gyration Rg and the scattering intensity at zero angle I(0) obtained by Guinier approximation are 19.0 Å and 0.16 cm^{-1}, respectively. The particle distance distribution function P(r) plots was calculated using GNOM (Svergun, 1992).

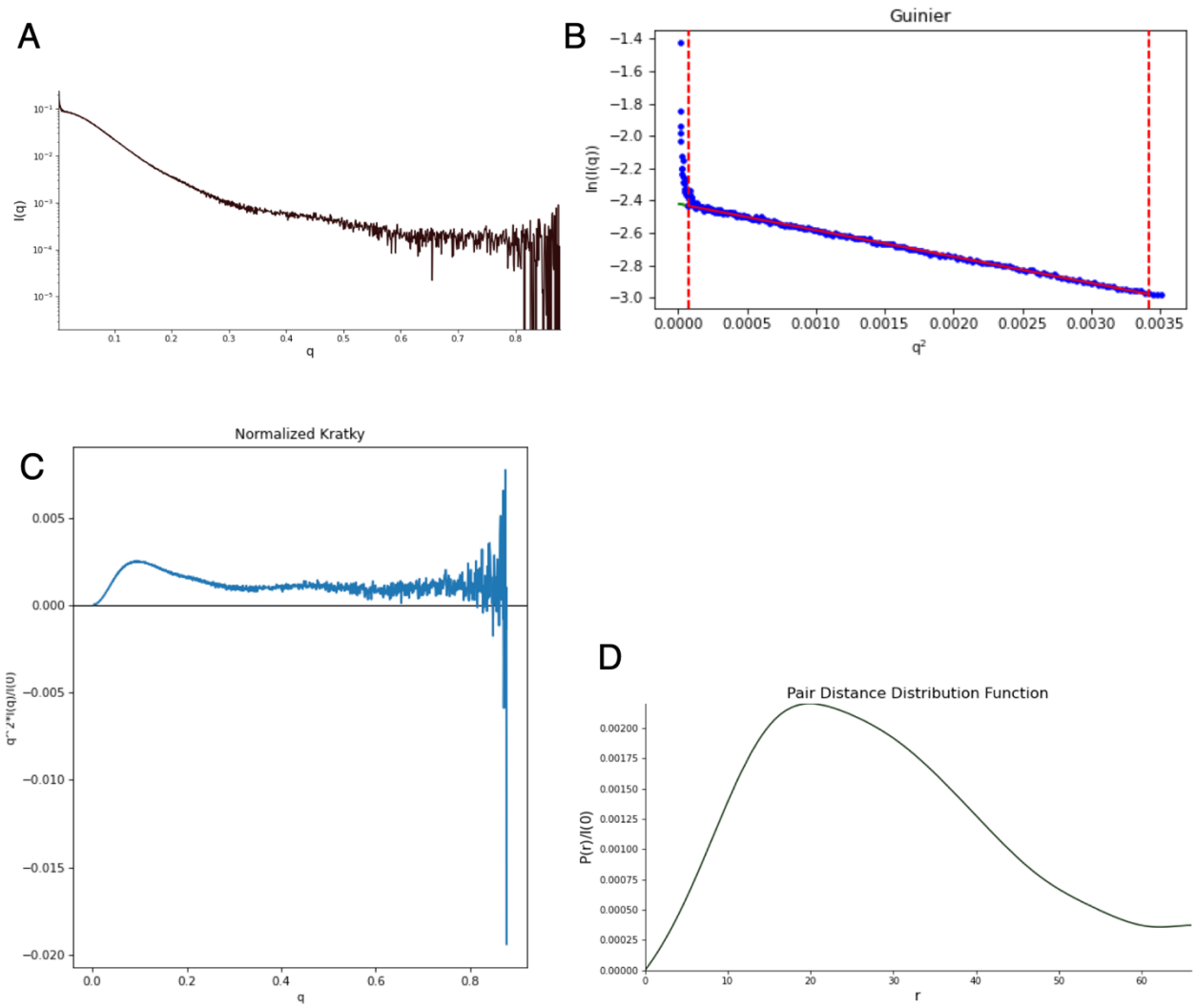

Supplementary Figure S15. Processed SAXS data of SLAshCUUG: (A) scattering curve; (B) Guinier approximation curve; (C) normalized Kratky plot; and (D) particle distance distribution function plot. The radius of gyration Rg and the scattering intensity at zero angle I(0) obtained by Guinier approximation are 22.1 Å and 0.09 cm^{-1}, respectively. The particle distance distribution function P(r) plots was calculated using GNOM (Svergun, 1992).

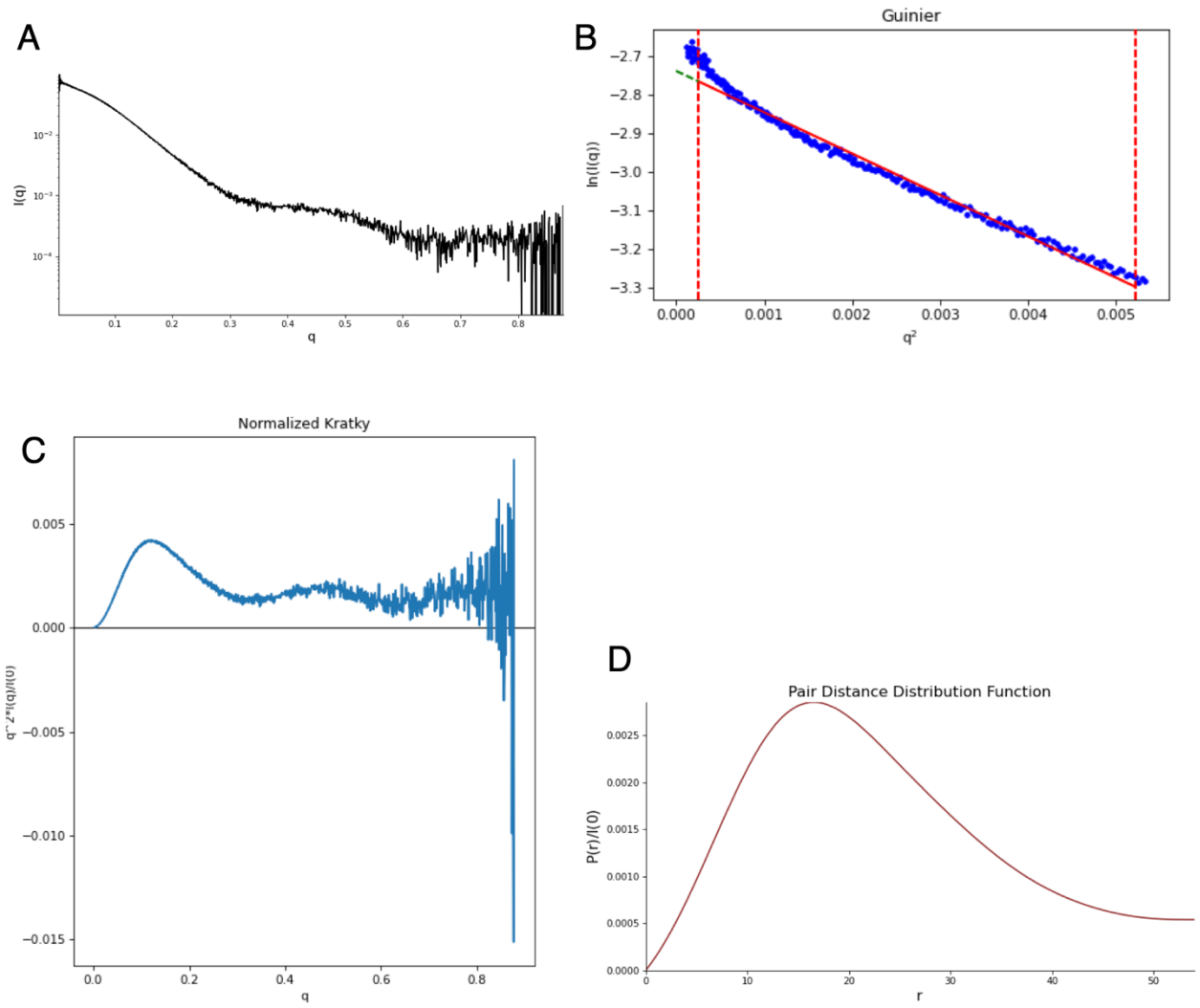

Supplementary Figure S16. Processed SAXS data of DenvSLATL: (A) scattering curve; (B) Guinier approximation curve; (C) normalized Kratky plot; and (D) particle distance distribution function plot. The radius of gyration Rg and the scattering intensity at zero angle I(0) obtained by Guinier approximation are 18.0 Å and 0.06 cm^{-1}, respectively. The particle distance distribution function P(r) plots was calculated using GNOM (Svergun, 1992).

References

Barnwal R. P., Loh E., Godin K. S., Yip J., Lavender H., Tang C. M., & Varani G. (2016). Structure and mechanism of a molecular rheostat, an RNA thermometer that modulates immune evasion by Neisseria meningitidis. *Nucleic Acids Res*, *44*(19), 9426-9437. https://doi.org/10.1093/nar/gkw584

Lee E., Bujalowski P. J., Teramoto T., Gottipati K., Scott S. D., Padmanabhan R., & Choi K. H. (2021). Structures of flavivirus RNA promoters suggest two binding modes with NS5 polymerase. *Nat Commun*, *12*(1), 2530. https://doi.org/10.1038/s41467-021-22846-1

Lodeiro M. F., Filomatori C. V., & Gamarnik A. V. (2009). Structural and functional studies of the promoter element for dengue virus RNA replication. *J Virol*, *83*(2), 993-1008. https://doi.org/10.1128/JVI.01647-08

Markham N. R., & Zuker M. (2008). UNAFold: software for nucleic acid folding and hybridization. *Methods Mol Biol*, *453*, 3-31. https://doi.org/10.1007/978-1-60327-429-6_1

Sharma S., & Varani G. (2020). NMR structure of Dengue West Nile viruses stem-loop B: A key cis-acting element for flavivirus replication. *Biochem Biophys Res Commun*, *531*(4), 522-527. https://doi.org/10.1016/j.bbrc.2020.07.115

Svergun D. I. (1992). Determination of the Regularization Parameter in Indirect-Transform Methods Using Perceptual Criteria. *Journal of Applied Crystallography*, *25*, 495-503. https://doi.org/Doi 10.1107/S0021889892001663

Walker M. J., Shortridge M. D., Albin D. D., Cominsky L. Y., & Varani G. (2020). Structure of the RNA Specialized Translation Initiation Element that Recruits eIF3 to the 5'-UTR of c-Jun. *J Mol Biol*, *432*(7), 1841-1855. https://doi.org/10.1016/j.jmb.2020.01.001

Zuker M. (2003). Mfold web server for nucleic acid folding and hybridization prediction. *Nucleic Acids Res*, *31*(13), 3406-3415. https://doi.org/10.1093/nar/gkg595